International Journal of Applied Engineering Research ISSN 0973-4562 Volume 14, Number 20 (2019) pp. 3935-3945

The Hall Currents and Ion Slip Effects on a Peristaltic MHD Nanofluid with Suspended Particles

Nabil T. M. El-dabe, Galal M. Moatimid[1], Mohamed A. Hassan[2] and Wessam A. Godh[3]

Department of Mathematics, Faculty of Education, Ain Shams University, Cairo, Egypt.

Abstract

This paper aims to studying the effects of the Hall currents, together with the wall properties and ion slip in magnetohydrodynamic (MHD) peristaltic transport of a nanofluid with suspended particles fluid through a porous medium. The mathematical formulation is presented for the fluid and the particle phases. The governing equations of motion were modeled under the constraints of low Reynolds number. The normal modes analysis was applied to relaxing the complexity of these equations. The analytic approximate solutions of these equations were obtained by using a perturbation method. The distributions of the velocities, stream function, nanoparticle concentration, temperature and pressure gradient were obtained. They were described through a set of graphs for various pertinent physical parameters. The effects of the Hall parameter and ion slip on the fluid reveal many interesting features, especially, on the pressure gradient profile. It was observed that when an ion slip parameter increases, the pressure gradient decreases in the middle of the channel. In contrast, in the wider part of the channel, this mechanism is reversed. The same influence of the Hall parameter of the pressure gradient was, also, seen.

Keywords: Nanofluid; Peristalsis; Slip conditions; Hall currents; Ion slip; Wall properties; Porous media; Normal modes analysis; Particle–fluid.

1. INTRODUCTION

Peristalsis is one of the major transport mechanism utilized for the fluid transportation in physiology. This mechanism contains waves of area contraction and relaxation which diffusing along the channel walls. In a living body, peristaltic flow happens because of simultaneous contraction and expansion of smooth muscles. An extensive variety of peristaltic flow can be observed in gastrointestinal tract (Chyme movement), cilia motion, movement of spermatozoa, vasomotion of small blood vessels and transportation of urine from the kidney to the bladder, In the recent years, this mechanism has been exploited in many industrial technologies including micro-pumps in pharmacology, heart–lung and dialysis machines and pumps used in transport of several corrosive and sensitive fluids in nuclear industry, toxic waste conveyance in chemical process engineering, magnetic endoscopy in gastric physiology, and most recently in rocket chamber fuel control technologies. Peristaltic transport of nanofluids is of significant significance in biomedical engineering, particularly in modern drug delivery systems, in hyperthermia and cryosurgery, which was used as a mean to medicate the malignancy. Abbasi et al. [1] studied the peristaltic motion of a non-Newtonian nanofluid in an asymmetric channel. They confirmed the fact that an increase in the Brownian motion parameter leads to the increase in haphazard motion of the nanoparticles which forbids them to settle at one place in the flow regime and consequently the concentration increases throughout the fluid. Shehzad et al. [2] studied the peristaltic motion of nanofluid with Joule heating and thermophoresis effects. They observed that the concentration of nanoparticles near the boundaries is enhanced for the larger thermophoresis parameter. However, the reverse situation is observed for an increase in the value of the Brownian motion parameter. Moreover, Hayat et al. [3] examined the peristaltic transport of nanofluid with Soret and Dufour effects. They have found that the pressure gradient attains its maximum value near the wider part of the channel and it decreases when moving towards the narrow part.

Nanofluids are engineered suspensions of nanometer-sized solid particles in a base fluid. The suspension of such particles enhances the thermo-physical properties (e.g. viscosity, density, and specific heat) of base fluids. Because of the unique chemical and mechanical properties, such fluids are easily being adopted in different industries to facilitate the heat transfer process. Nanofluids have applications in biomedical engineering, automobile, domestic cooling, nuclear reactors; for instance, see Refs. [4,5]. Because of their growing application as of late, several researchers performed experimental and numerical studies to investigate the application of nanofluids to control heat transfer in a process. Khan et al. [6] discussed the unsteady flow of Eyring Powell fluid over a porous oscillatory stretching sheet in the presence of nano particles. Their study revealed that the velocity increases by increasing fluid parameter, while the presence of porosity parameter and Hartmann number resist the motion of the fluid. Hayat et al. [7] studied the three-dimensional boundary layer flow of viscous nanofluid. They investigated that there is an enhancement in the concentration profile when the Schmidt number increases.

[1] E-mail address: gal_moa @ hotmail.com.
[2] E-mail address: m_a_Hassan_gk @ hotmail.com.
[3] E-mail address: al_ostaz_y2k @ yahoo.com.

The flow of particulate suspension is significance on the grounds that it is helpful in propagating biological fluids in a human body that happens due to peristaltic wave and acts like fluid-particle mixture. Utilizing the continuum approach, the investigation of particle-fluid is especially applicable in the hydrodynamics of biological systems, since it is helpful to explore numerous subjects; for instance, capillary hemodynamic flow in vivo, fluidization, and sedimentation [8, 9]. It is also notable that the anisotropic particle microstructures and the clusters are the results of particle movement that happens because of wall-particle and particle-particle collision [10]. Feng et al. [11] presented a two-dimensional numerical study of the viscoelastic effects on the sedimentation of particles in the presence of solid walls or another particle. They concluded that the particle-particle interactions are in qualitative agreement with the experimental observations. Meanwhile, the wall repulsion has not been documented in experiments.

Hall and ion slip currents have noteworthy impacts for a strong magnetic field as in MHD flows where electromagnetic force is remarkable. These effects have abundant applications in various fields which encompass the devices like power generators, Hall accelerators, transformers, magnetometers to measure the magnetic field, refrigeration coils, electric transformers, and spacecraft propulsion. Therefore, Abo-Eldahab et al. [12] studied the Hall and ion-slip effects on peristalsis of viscous fluid. They observed that both the mean velocity and the flow reveal decreases with an increase in the Hall and ion slip parameters, and increases with the increasing of the electric conductivity, and imposed magnetic field. Srinivasacharya and Kaladhar [13] analyzed the analytical solution of the Hall and ion slip effects on mixed convection flow of couple stress fluid. They concluded that the increase in the Hall and ion slip parameters leads to decrease in the radial and axial velocities. Uddin and Kumar [14] addressed the influences of the Hall and ion slip on the MHD boundary layer flow of micropolar fluid. Their results show that the local skin friction coefficient, due to translational motion, increases with the angle of the wedge and Hall parameter. Therefore, heat transfer rate increases with these parameters. Hayat et al. [15] investigated the effects of the Hall current and chemical reaction on the mixed convective peristaltic flow of Prandtl fluid. Their results show that the concentration increases in the presence of a chemical reaction. Opposite impacts of the Hartman number and Hall parameter are observed for velocity.

A significant role in multiphase problems was played by slip conditions. The impacts of slip condition are catheterized as fluid involves of rare field gases or because of flexible features [16]. The idea of the slip of a fluid at a solid wall served to describe macroscopic impacts of certain molecular phenomena. The vast majority of investigations in all studies on peristaltic flow are centered around situations, including the classical Navier–Stokes at no slip condition. Nevertheless, a few investigations, studies the incorporating slip flow has been displayed in the recent years. In order to investigate the effect of the slip condition on nanofluid flow, a study has been carried out by Abedin et al. [17]. They considering the slip boundary conditions. The important results of this study indicated that the enhancement of volume fraction of nanoparticles, Reynolds number and dimensionless slip velocity coefficient cause a considerable augmentation of heat transfer and reduction in thermal resistance of the surface. Soltani and Yilmazer [18] studied the slip effects and slip layer thickness propagating in a concentrated suspension. In this study, the flow of highly filled suspensions was strongly affected by slip at the wall. Slip velocity was found to vary linearly with shear stress at the wall. Slip velocity values increased with increasing temperature.

The flow in a compliant channel has various physiological applications; for instance, urine stream in the urethras, air flow in the lungs, and blood flow in arteries and veins. Hayat et al. [19] considered the effect of the wall properties and slip on the peristaltic motion of nanofluid with MHD and Joule heating. They observed that the velocity gives an increasing function of the wall rigidity parameter and the wall tension. Moreover, it decreases with an increase in the mass characterization parameter. Furthermore, it is observed that the velocity profile is parabolic for fixed values of parameters and its magnitude is maximum near the center of the channel. Shahzadi et al. [20] made a bio-mathematical investigation of the peristaltic flow of single-wall carbon nanotubes under the effect of variable viscosity and wall properties. They investigated that the trapping phenomena show that the size of the trapped bolus is smaller for a pure blood case as compared to the single-wall carbon nanotubes.

In light of the above discussion, the objective of the current paper is to analyze the effects of the Hall current, ion slip and slip conditions on a MHD peristaltic transport of particulate fluid suspended in a nanofluid. The wall properties and the permeability of the channel were taken into account. The analysis is performed under low Reynolds number approximation. The normal modes analysis of the governing equations for the fluid phase and the particulate phase was analyzed. The resulting equations are analytically solved by using a perturbation technique. The approximate distributions of the stream function, fluid and particles velocities, concentration, temperature and pressure gradient was derived. All the physical features of the problems have been described throughout a set of graphs.

2. FORMULATION OF THE PROBLEM

A two-dimensional flexible permeable channel of uniform thickness was considered. It was filled with a mixture of small spherical rigid particles in an incompressible Newtonian viscous fluid. The following assumptions are considered:

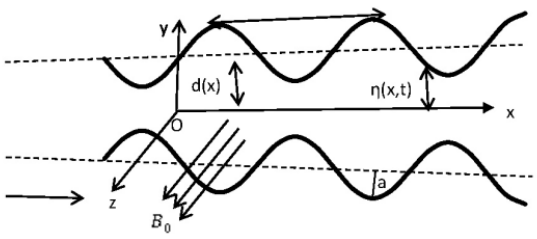

Fig. 1 Geometry of the problem.

- The characteristic properties of the two-dimensional flow depend on the two-dimensions in the Cartesian coordinates (x, y), where the flow direction was horizontally taken in the x-axis and the y-axis is vertical.
- A viscous Newtonian incompressible nanofluid flow is assumed.
- For simplicity, an axisymmetric type of motion is cnsidered, the gravitational forces are neglected under the assumption of horizontal motion as a facilitator of the solution.
- Extra simplified presumptions about the movement of the suspended particles, which are taken to be monodisperse and solid spherical particles [21] are considered.
- The bulk concentration of the particles is assumed to be very small (i.e. concentration by volume). Therefore, the net effect of the particles on the fluid is equivalent to an extra force $\gamma\zeta(\underline{V}_p - \underline{V})$ per unit volume [21].
- The Hall currents and ion slip effects were taken into account by applying a strong uniform magnetic field with magnetic flux density $\underline{B} = (0,0,B_0)$.

The description of the problem is sketched in Fig.1 along the above considerations.

The channel wall geometry is represented as:

$$\eta(x,t) = d(x) + a\sin\frac{2\pi}{\lambda^*}(x - c^*t), \quad (1)$$

where $d(x) = d + Q^*x, \quad Q^* << 1.$

If the Hall and ion slip terms are retained in the generalized Ohm's law, then the current density $\underline{J}$ is given by [22, 23]

$$\underline{J} = \sigma\left(\underline{E} + \underline{V}\times\underline{B} - \beta^*(\underline{J}\times\underline{B}) + \frac{\beta^*\beta_i}{B_0}(\underline{J}\times\underline{B})\times\underline{B}\right), \quad (2)$$

Where $\underline{E}$ is the electric field which results from a charge separation in the z-direction, β^* is the Hall factor, and β_i is the ion slip parameter [22, 23].

Under the previous assumptions, the basic equations that are governing the motion become

- **Fluid phase:**

The incompressibility conditions, yields

$$\frac{\partial u}{\partial x} + \frac{\partial v}{\partial y} = 0, \quad (3)$$

The conversation of momentum, gives

$$\rho\left[\frac{\partial u}{\partial t} + u\frac{\partial u}{\partial x} + v\frac{\partial u}{\partial y}\right] = -\frac{\partial p}{\partial x} + \mu\left[\frac{\partial^2 u}{\partial x^2} + \frac{\partial^2 u}{\partial y^2}\right] - \frac{\mu}{K}u - \frac{\sigma B_0^2(1+\beta_i\beta_e)u}{(1+\beta_i\beta_e)^2+\beta_e^2} + \frac{(\sigma B_0^2\beta_e\beta^*)v}{(1+\beta_i\beta_e)^2+\beta_e^2} - \gamma\zeta\,(u_p - u), \quad (4)$$

and

$$\rho\left[\frac{\partial v}{\partial t} + u\frac{\partial v}{\partial x} + v\frac{\partial v}{\partial y}\right] = -\frac{\partial p}{\partial y} + \mu\left[\frac{\partial^2 v}{\partial x^2} + \frac{\partial^2 v}{\partial y^2}\right] - \frac{\mu}{K}v - \frac{\sigma B_0^2(1+\beta_i\beta_e)v}{(1+\beta_i\beta_e)^2+\beta_e^2} + \frac{(\sigma B_0^2\beta_e\beta^*)u}{(1+\beta_i\beta_e)^2+\beta_e^2} - \gamma\zeta(v_p - v), \quad (5)$$

The conversation of energy, results

$$\frac{\partial T}{\partial t} + u\frac{\partial T}{\partial x} + v\frac{\partial T}{\partial y} = \left(\frac{k}{\rho c_f}\right)\left[\frac{\partial^2 T}{\partial x^2} + \frac{\partial^2 T}{\partial y^2}\right] + \left(\frac{\rho_p c_p}{\rho c_f}\right)\left[D_B\left(\frac{\partial C}{\partial x}\frac{\partial T}{\partial x} + \frac{\partial C}{\partial y}\frac{\partial T}{\partial y}\right) + \frac{D_T}{T_0}\left(\left(\frac{\partial T}{\partial x}\right)^2 + \left(\frac{\partial T}{\partial y}\right)^2\right)\right], \quad (6)$$

Finally, the concentration equation, presents

$$\frac{\partial C}{\partial t} + u\frac{\partial C}{\partial x} + v\frac{\partial C}{\partial y} = D_B\left(\frac{\partial^2 C}{\partial x^2} + \frac{\partial^2 C}{\partial y^2}\right) + \frac{D_T}{T_0}\left(\frac{\partial^2 T}{\partial x^2} + \frac{\partial^2 T}{\partial y^2}\right), \quad (7)$$

- **Particulate phase**:

The equations of motion and continuity for the particles are given by[21]:

$$m\zeta\left[\frac{\partial u_p}{\partial t} + u_p\frac{\partial u_p}{\partial x} + v_p\frac{\partial u_p}{\partial y}\right] = \gamma\zeta(u - u_p), \quad (8)$$

$$m\zeta\left[\frac{\partial v_p}{\partial t} + u_p\frac{\partial v_p}{\partial x} + v_p\frac{\partial v_p}{\partial y}\right] = \gamma\zeta(v - v_p), \quad (9)$$

and

$$\frac{\partial \zeta}{\partial t} + \frac{\partial \zeta u_p}{\partial x} + \frac{\partial \zeta v_p}{\partial y} = 0, \quad (10)$$

where $m\zeta$ is equivalent to the mass of particles per unit volume (the buoyancy force is neglected), and $\beta_e = \sigma\beta^* B_0$ is the Hall parameter [21].

In accordance with the axisymmetric motion of the flexible wall, the theory of a stretched membrane with a viscous damping force is considered. Mitra and Prasad [24] suggested the dynamic boundary conditions $\frac{\partial}{\partial x}L^*(\eta) = \frac{\partial p}{\partial x}$ at $y = \pm\eta(x,t)$, where $L^*(\eta) = p - p_0$, and L^* is an operator, which is used to represent the motion of a stretched membrane with viscosity damping forces such that

$L^* = -\tau\frac{\partial^2}{\partial x^2} + m_1^*\frac{\partial^2}{\partial t^2} + C_v\frac{\partial}{\partial t}$, τ is the elastic tension in the membrane, m_1^* is the mass per unit area, C_v is the coefficient of viscous damping forces and p_0 is the pressure on the outside surface of the wall due to tension in the muscles. This tension may be obtained through the constitutive relation of the muscles when the displacements are known. For simplicity, we may ignore the parameter p_0 [25].

Using Eq. (4), we get the compliant wall condition as:

$$\frac{\partial}{\partial x}L^*(\eta) = \frac{\partial p}{\partial x} = \mu\left[\frac{\partial^2 u}{\partial x^2} + \frac{\partial^2 u}{\partial y^2}\right] - \rho\left[\frac{\partial u}{\partial t} + u\frac{\partial u}{\partial x} + v\frac{\partial u}{\partial y}\right] - \frac{\mu}{K}u - \frac{\sigma B_0^2(1+\beta_i\beta_e)u}{(1+\beta_i\beta_e)^2+\beta_e^2} + \frac{(\sigma B_0^2\beta_e\beta^*)v}{(1+\beta_i\beta_e)^2+\beta_e^2} - \gamma\zeta(u_p - u), \quad (11)$$

(at $y = \pm\eta$)

For the adequately small particles, the velocity of sedimentation will be small compared with a characteristic velocity of the flow and can be neglected. Therefore, in a steady state, the inertia terms in the equation of motion vanish identically and the particles move along the streamlines with the velocity of the fluid (i.e. $\underline{V} = \underline{V_p}$ at $y = 0$). The density number ζ is constant along the streamlines. So, suppose that it has a constant value ζ everywhere [21].

To complete the formulation of boundary-value problem, the appropriate boundary conditions, may be listed as follows:

$T = T_0$, $C = C_0$, $v = \frac{\partial \eta}{\partial t}$ at $y = -\eta(x,t)$, and $T = T_1$, $C = C_1$, $v = -\frac{\partial \eta}{\partial t}$ at $y = -\eta(x,t)$.

In addition, one finds $u = u_p$, and $v = v_p$ at $y = 0$. [21].

The slip conditions at the walls are defined as:

$$u = \mp h \frac{\partial u}{\partial y} \text{ at } y = \pm\eta(x,t) = \pm\left[d + Q^* x + a\sin\frac{2\pi}{\lambda^*}(x - c^* t)\right], \quad (12)$$

Now, it is convenient to introduce the following non-dimensional quantities:

$$x' = \frac{x}{\lambda^*},\ y' = \frac{y}{d}, u' = \frac{u}{c}, v' = \frac{v}{\delta c},\ t' = \frac{ct}{\lambda^*}, w = \frac{mc}{\lambda^* \gamma},\ L = \frac{mcd^2\zeta}{\mu\lambda^*}, \Omega = \frac{C - C_0}{C_1 - C_0},$$

$$\theta = \frac{T - T_0}{T_1 - T_0}, \eta' = \frac{\eta}{d},\ p' = \frac{d^2 p}{c^* \lambda^* \mu},\ K' = \frac{K}{d^2},\ \alpha = \frac{k}{\rho c_f},\ N_b = \frac{\rho c_p D_B (C_1 - C_0)}{\rho c_f \alpha}, \beta = \frac{h}{d}, \varepsilon = \frac{a}{d},\ N_t = \frac{\rho c_p D_T (T_1 - T_0)}{\rho c_f \alpha T_0},\ M^2 = \frac{\sigma B_0^2 d^2}{\mu},\ \nu = \frac{\mu}{\rho},\ Pr = \frac{\nu}{\alpha},\ Sc = \frac{\nu}{D_B},\ R = \frac{c^* d\rho}{\mu}, \delta = \frac{d}{\lambda^*},$$

$$E_1 = \frac{-\tau d^3}{\lambda^{*3}\mu c^*}, E_2 = \frac{m_1^* c^* d^3}{\lambda^{*3}\mu}, E_3 = \frac{C_v d^3}{\lambda^{*2}\mu} \text{ and } Q = \frac{\lambda^* Q^*}{d}. \quad (13)$$

Using the above non-dimensional quantities in equations $(1) - (13)$ under the assumptions of the low Reynolds number approximations, the resulting equations of the fluid phase can be written as:

$$\eta(x,t) = 1 + Qx + \varepsilon \sin 2\pi(x - t), \quad (14)$$

- **Fluid phase:**

$$\frac{\partial u}{\partial x} + \frac{\partial v}{\partial y} = 0, \quad (15)$$

$$\frac{\partial p}{\partial x} = \delta^2 \frac{\partial^2 u}{\partial x^2} + \frac{\partial^2 u}{\partial y^2} + \left(\frac{L}{w} - \frac{1}{k} - M^2\left(\frac{(1+\beta_i\beta_e)}{(1+\beta_i\beta_e)^2 + \beta_e^2}\right)\right) u + M^2\left(\frac{\delta(\beta^*\beta_e)}{(1+\beta_i\beta_e)^2+\beta_e^2}\right) v - \frac{L}{w} u_p, \quad (16)$$

$$\frac{\partial p}{\partial y} = \delta^2\left[\delta^2 \frac{\partial^2 v}{\partial x^2} + \frac{\partial^2 v}{\partial y^2}\right] - \delta^2\left(\frac{1}{K} - \frac{L}{w} + M^2\left(\frac{(1+\beta_i\beta_e)}{(1+\beta_i\beta_e)^2+\beta_e^2}\right)\right) v + M^2\left(\frac{\delta(\beta^*\beta_e)}{(1+\beta_i\beta_e)^2+\beta_e^2}\right) u - \delta^2 \frac{L}{w} v_p, \quad (17)$$

$$\delta^2\left[\frac{\partial^2\theta}{\partial x^2} + N_b \frac{\partial\Omega}{\partial x}\frac{\partial\theta}{\partial x} + N_t\left(\frac{\partial\theta}{\partial x}\right)^2\right] + \left[\frac{\partial^2\theta}{\partial y^2} + N_b \frac{\partial\Omega}{\partial y}\frac{\partial\theta}{\partial y} + N_t\left(\frac{\partial\theta}{\partial y}\right)^2\right] = 0, \quad (18)$$

and

$$\delta^2\left[\frac{\partial^2\Omega}{\partial x^2} + \frac{N_t}{N_b}\frac{\partial^2\theta}{\partial x^2}\right] + \left[\frac{\partial^2\Omega}{\partial y^2} + \frac{N_t}{N_b}\frac{\partial^2\theta}{\partial y^2}\right] = 0. \quad (19)$$

- **For the particulate phase, it can be written as:**

$$\frac{\partial u_p}{\partial x} + \frac{\partial v_p}{\partial y} = 0, \quad (20)$$

$$w\left[\frac{\partial u_p}{\partial t} + u_p \frac{\partial u_p}{\partial x} + v_p \frac{\partial u_p}{\partial y}\right] = u - u_p \quad (21)$$

and

$$w\left[\frac{\partial v_p}{\partial t} + u_p \frac{\partial v_p}{\partial x} + \delta v_p \frac{\partial v_p}{\partial y}\right] = v - v_p \quad (22)$$

- **In addition, the related boundary conditions yield:**

$$u = \mp\beta \frac{\partial u}{\partial y} \text{ and } v = \pm\frac{\partial \eta}{\partial t} \quad at \quad y = \pm\eta(x,t) = \pm[1 + Qx + \varepsilon \sin 2\pi(x - t)], \quad (23)$$

$$\delta^2 \frac{\partial^2 u}{\partial x^2} + \frac{\partial^2 u}{\partial y^2} + \left(\frac{L}{w} - \frac{1}{k} - M^2\left(\frac{(1+\beta_i\beta_e)}{(1+\beta_i\beta_e)^2+\beta_e^2}\right)\right) u + M^2\left(\frac{\delta(\beta^*\beta_e)}{(1+\beta_i\beta_e)^2+\beta_e^2}\right) v - \frac{L}{w} u_p = -8\varepsilon\pi^3(E_1 + E_2)\cos 2\pi(x - t) + 4\varepsilon\pi^2 E_3 \sin 2\pi(x - t), \quad at\ y = \pm\eta(x,t) \quad (24)$$

$$\left.\begin{array}{l} \theta(x,y,t) = \Omega(x,y,t) = 0, at\ y = -\eta(x,t) \\ \theta(x,y,t) = \Omega(x,y,t) = 1, at \quad y = \eta(x,t) \\ u = u_p, \text{ and } \quad v = v_p, \text{at } y = 0 \end{array}\right\} \quad (25)$$

where $N^2 = M^2 + \frac{1}{K}$. Now, the previous system of equations $(14) - (25)$ will be solved in the next sections.

3. METHOD OF SOLUTION

It should be noted that the previous equations seemed impossible to find the solution in closed form for the arbitrary values of all parameters. Even for the Newtonian fluids, all analytical solutions were obtained so far were based on the assumption that one or several parameters were zero or small. For the solution of Eqs. (15−22) in light of the boundary conditions (23−25), the perturbation method depending on the long wave assumption is assumed. For that the functions $u_p, v_p, u, v, p, \theta$ and Ω may be expanded as follows [26]:

$$f = f_0 + \delta f_1 + \delta^2 f_2 + \cdots \quad (26)$$

Inserting Eq. (26) into Eqs. (15−22) and (23−25) and then collecting the terms of equal powers of δ one obtains the following systems:

3.1. Zero-order system

$$\frac{\partial u_0}{\partial x} + \frac{\partial v_0}{\partial y} = 0, \quad (27)$$

$$\frac{\partial p_0}{\partial x} = \frac{\partial^2 \mathrm{u}_0}{\partial \mathrm{y}^2} + \mathrm{c}_1 \mathrm{u}_0 - \mathrm{c}_2 u_{p_0}, \tag{28}$$

$$\frac{\partial p_0}{\partial y} = 0, \tag{29}$$

$$\frac{\partial^2 \theta_0}{\partial \mathrm{y}^2} + \mathrm{N_b} \frac{\partial \Omega_0}{\partial \mathrm{y}} \frac{\partial \theta_0}{\partial \mathrm{y}} + \mathrm{N_t} \left(\frac{\partial \theta_0}{\partial \mathrm{y}}\right)^2 = 0, \tag{30}$$

$$\frac{\partial^2 \Omega_0}{\partial \mathrm{y}^2} + \frac{\mathrm{N_t}}{\mathrm{N_b}} \frac{\partial^2 \theta_0}{\partial \mathrm{y}^2} = 0. \tag{31}$$

$$\frac{\partial u_{p_0}}{\partial x} + \frac{\partial v_{p_0}}{\partial y} = 0, \tag{32}$$

$$w\left[\frac{\partial \mathrm{u_{p_0}}}{\partial \mathrm{t}} + \mathrm{u_{p_0}} \frac{\partial \mathrm{u_{p_0}}}{\partial \mathrm{x}} + \mathrm{v_{p_0}} \frac{\partial \mathrm{u_{p_0}}}{\partial \mathrm{y}}\right] = u_0 - \mathrm{u_{p_0}}\ , \tag{33}$$

$$w\left[\frac{\partial \mathrm{v_{p_0}}}{\partial \mathrm{t}} + \mathrm{u_{p_0}} \frac{\partial \mathrm{v_{p_0}}}{\partial \mathrm{x}}\right] = v_0 - \mathrm{v_{p_0}}, \tag{34}$$

and the related boundary conditions yield:

$$u_0 = \mp\beta \frac{\partial \mathrm{u_0}}{\partial y} \ and\ v_0 = \pm \frac{\partial \eta}{\partial t} \ at\ y = \pm\eta(x,t) = \pm[1 + Qx + \varepsilon \sin 2\pi(x - t)], \tag{35}$$

$$\frac{\partial^2 \mathrm{u_0}}{\partial \mathrm{y}^2} + \mathrm{c}_1 \mathrm{u}_0 - \mathrm{c}_2 u_{p_0} = \mathrm{c}_3 \cos 2\pi(\mathrm{x} - \mathrm{t}) + \mathrm{c}_4 \sin 2\pi(\mathrm{x} - \mathrm{t}), \quad \text{at } y = \pm\eta(x,t) \tag{36}$$

$$\left.\begin{array}{l} \theta_0(x,y,t) = \Omega_0(x,y,t) = 0, \quad at\ y = -\eta(x,t) \\ \theta_0(x,y,t) = \Omega_0(x,y,t) = 1, \quad at \quad y = \eta(x,t) \\ u_0 = u_{p_0}, \text{ and } \quad v_0 = v_{p_0}, \text{at } y = 0 \end{array}\right\} \tag{37}$$

3.2. First-order system

$$\frac{\partial u_1}{\partial x} + \frac{\partial v_1}{\partial y} = 0, \tag{38}$$

$$\frac{\partial p_1}{\partial x} = \frac{\partial^2 \mathrm{u}_1}{\partial \mathrm{y}^2} + \mathrm{c}_1 \mathrm{u}_1 + \mathrm{c}_5 \mathrm{v}_0 - \mathrm{c}_2 u_{p_1}, \tag{39}$$

$$\frac{\partial p_1}{\partial y} = \mathrm{c}_5 \mathrm{u}_0, \tag{40}$$

$$\frac{\partial^2 \theta_1}{\partial \mathrm{y}^2} + \mathrm{N_b}\left(\frac{\partial \Omega_0}{\partial \mathrm{y}} \frac{\partial \theta_1}{\partial \mathrm{y}} + \frac{\partial \Omega_1}{\partial \mathrm{y}} \frac{\partial \theta_0}{\partial \mathrm{y}}\right) + 2\mathrm{N_t} \frac{\partial \theta_0}{\partial \mathrm{y}} \frac{\partial \theta_1}{\partial \mathrm{y}} = 0, \tag{41}$$

$$\frac{\partial^2 \Omega_1}{\partial \mathrm{y}^2} + \frac{\mathrm{N_t}}{\mathrm{N_b}} \frac{\partial^2 \theta_1}{\partial \mathrm{y}^2} = 0. \tag{42}$$

$$\frac{\partial u_{p_1}}{\partial x} + \frac{\partial v_{p_1}}{\partial y} = 0, \tag{43}$$

$$w\left[\frac{\partial \mathrm{u_{p_1}}}{\partial \mathrm{t}} + \mathrm{u_{p_1}} \frac{\partial \mathrm{u_{p_0}}}{\partial \mathrm{x}} + \mathrm{u_{p_0}} \frac{\partial \mathrm{u_{p_1}}}{\partial \mathrm{x}} + \mathrm{v_{p_1}} \frac{\partial \mathrm{u_{p_0}}}{\partial \mathrm{y}} + \mathrm{v_{p_0}} \frac{\partial \mathrm{u_{p_1}}}{\partial \mathrm{y}}\right] = u_1 - \mathrm{u_{p_1}}\ , \tag{44}$$

$$w\left[\frac{\partial \mathrm{v_{p_1}}}{\partial \mathrm{t}} + \mathrm{u_{p_1}} \frac{\partial \mathrm{v_{p_0}}}{\partial \mathrm{x}} + \mathrm{u_{p_0}} \frac{\partial \mathrm{v_{p_1}}}{\partial \mathrm{x}} + \mathrm{v_{p_0}} \frac{\partial \mathrm{v_{p_0}}}{\partial \mathrm{x}}\right] = v_1 - \mathrm{v_{p_1}}, \tag{45}$$

and the related boundary conditions yield:

$$u_1 = \mp\beta \frac{\partial \mathrm{u_1}}{\partial y} \ and\ v_1 = 0 \ \ at\ y = \pm\eta(x,t) = \pm[1 + Qx + \varepsilon \sin 2\pi(x - t)], \tag{46}$$

$$\frac{\partial^2 \mathrm{u_0}}{\partial \mathrm{y}^2} + \mathrm{c}_1 \mathrm{u}_1 + \mathrm{c}_5 \mathrm{v}_0 - \mathrm{c}_2 u_{p_1} = 0, \quad \text{at } y = \pm\eta(x,t) \tag{47}$$

$$\left.\begin{array}{l} \theta_1(x,y,t) = \Omega_1(x,y,t) = 0, \quad at\ y = -\eta(x,t) \\ \theta_1(x,y,t) = \Omega_1(x,y,t) = 0, \quad at \quad y = \eta(x,t) \\ u_1 = u_{p_1}, \text{ and } \quad v_1 = v_{p_1}, \text{at } y = 0 \end{array}\right\} \tag{48}$$

Now our interest lies in the solutions of the above systems.

3.3. Zero-order solution

The elimination of the variable u_0 between equations (28), (33) and differentiation of the result equation partially with respect to y yield the following equation:

$$(c_1 - c_2)\frac{\partial \mathrm{u_{p_0}}}{\partial y} + \frac{\partial^4 \mathrm{u_{p_0}}}{\partial y^3 \partial t} + w\frac{\partial^3 \mathrm{u_{p_0}}}{\partial y^3}\frac{\partial \mathrm{u_{p_0}}}{\partial x} + 3w\frac{\partial^2 \mathrm{u_{p_0}}}{\partial y^2}\frac{\partial^2 \mathrm{u_{p_0}}}{\partial x \partial y} + 3w\frac{\partial \mathrm{u_{p_0}}}{\partial y}\frac{\partial^3 \mathrm{u_{p_0}}}{\partial y^2 \partial x} + w\mathrm{u_{p_0}}\frac{\partial^4 \mathrm{u_{p_0}}}{\partial y^3 \partial x} + w\frac{\partial^3 \mathrm{v_{p_0}}}{\partial y^3}\frac{\partial \mathrm{u_{p_0}}}{\partial y} + 3w\frac{\partial^2 \mathrm{v_{p_0}}}{\partial y^2}\frac{\partial^2 \mathrm{u_{p_0}}}{\partial y^2} + 3w\frac{\partial \mathrm{v_{p_0}}}{\partial y}\frac{\partial^3 \mathrm{u_{p_0}}}{\partial y^3} + w\mathrm{v_{p_0}}\frac{\partial^4 \mathrm{u_{p_0}}}{\partial y^4} + \frac{\partial^3 \mathrm{u_{p_0}}}{\partial y^3} + c_1 w\frac{\partial^2 \mathrm{u_{p_0}}}{\partial y \partial t} + c_1 w\frac{\partial \mathrm{u_{p_0}}}{\partial y}\frac{\partial \mathrm{u_{p_0}}}{\partial x} + c_1 w\mathrm{u_{p_0}}\frac{\partial^2 \mathrm{u_{p_0}}}{\partial y \partial x} + c_1 w\frac{\partial \mathrm{v_{p_0}}}{\partial y}\frac{\partial \mathrm{u_{p_0}}}{\partial y} + c_1 w\mathrm{v_{p_0}}\frac{\partial^2 \mathrm{u_{p_0}}}{\partial y^2} = 0, \tag{49}$$

The elimination of u_0 and v_0 from equations (28), (33) and (34), yield the following equation:

$$w\frac{\partial^2 \mathrm{u_{p_0}}}{\partial x \partial t} + w\frac{\partial^2 \mathrm{v_{p_0}}}{\partial y \partial t} + w\frac{\partial^2 \mathrm{u_{p_0}}}{\partial x^2} + w\mathrm{u_{p_0}}\frac{\partial^2 \mathrm{u_{p_0}}}{\partial x^2} + 2w\frac{\partial \mathrm{u_{p_0}}}{\partial y}\frac{\partial \mathrm{v_{p_0}}}{\partial x} + w\mathrm{v_{p_0}}\frac{\partial^2 \mathrm{u_{p_0}}}{\partial x \partial y} + w\mathrm{u_{p_0}}\frac{\partial^2 \mathrm{v_{p_0}}}{\partial x \partial y} = 0, \tag{50}$$

The solutions for $\mathrm{u_{p_0}}, \mathrm{v_{p_0}}, \mathrm{u_0}, \mathrm{v_0}, \theta_0, \Omega_0$ and p_0 may be obtained by using the normal mode analysis [27]:

$$g(x,y,t) = g^*(y)e^{i\lambda(x-t)} + \mathrm{c.c.}, \tag{51}$$

($c.c.$ means the complex conjugate of the preceding term).

Substituting from Eqs. (51) into Eqs. (27) − (37), (50) and equating the coefficient of $e^{i\lambda(x-t)}$ then by solving the resulting ordinary differential equations to find $g^*(y)$ and finally, using (51), one gets

$$\mathrm{u_{p_0}}(x,y,t) = \left(k_3 + k_4 \sin(\sqrt{\frac{k_1}{k_2}}y) + k_5 \cos(\sqrt{\frac{k_1}{k_2}}y)\right)e^{i\lambda(x-t)} \tag{52}$$

$$\mathrm{v_{p_0}}(x,y,t) = \left(-i\lambda k_3 y + i\lambda k_4\sqrt{\frac{k_2}{k_1}}\cos(\sqrt{\frac{k_1}{k_2}})y - i\lambda k_5\sqrt{\frac{k_2}{k_1}}\sin(\sqrt{\frac{k_1}{k_2}}y) + k_6\right)e^{i\lambda(x-t)} \tag{53}$$

$$\mathrm{u_0}(x,y,t) = (k_7\sin(\sqrt{c_1}y) + k_8\cos(\sqrt{c_1}y) + \frac{c_2}{c_1 - \frac{k_1}{k_2}}k_4\sin(\sqrt{\frac{k_1}{k_2}}y) + \frac{c_2}{c_1 - \frac{k_1}{k_2}}k_5\cos(\sqrt{\frac{k_1}{k_2}}y) + \frac{i\lambda p_0 + c_2 k_2}{c_1})e^{i\lambda(x-t)} \tag{54}$$

$$\mathrm{v_0}(x,y,t) = k_2(-i\lambda k_3 y + i\lambda\sqrt{\frac{k_2}{k_1}}k_4\cos\left(\sqrt{\frac{k_1}{k_2}}y\right) - i\lambda\sqrt{\frac{k_2}{k_1}}k_5\sin(\sqrt{\frac{k_1}{k_2}}y) + k_6)e^{i\lambda(x-t)} \tag{55}$$

$$\theta_0(x,y,t) = (k_9 y + k_{10})e^{i\lambda(x-t)} \quad (56)$$

$$\Omega_0(x,y,t) = (k_{11} y + k_{12})e^{i\lambda(x-t)} \quad (57)$$

$$p_0(x,t) = \frac{-i}{\lambda}(c_3 \cos 2\pi(x-t) + c_4 \sin 2\pi(x-t))e^{-i\lambda(x-t)} \quad (58)$$

By introducing a stream function ψ_0 and as $u_0 = \frac{\partial \psi_0}{\partial y}$ (59)

So, the stream function may be evaluated numerically by using the Mathematica software.

3.4. First order solution

The elimination of the variable p_1 between equations (39), (44) yields the following equation:

$$c_5 \frac{\partial u_0}{\partial x} - c_5 \frac{\partial v_0}{\partial y} + c_2 \frac{\partial u_{p_1}}{\partial y} = w \frac{\partial^4 u_{p_1}}{\partial y^3 \partial t} + w \frac{\partial^3 u_{p_1}}{\partial y^3} \frac{\partial u_{p_0}}{\partial x} +$$
$$3w \frac{\partial^2 u_{p_1}}{\partial y^2} \frac{\partial^2 u_{p_0}}{\partial x \partial y} + 3w \frac{\partial u_{p_1}}{\partial y} \frac{\partial^3 u_{p_0}}{\partial y^2 \partial x} + w u_{p_1} \frac{\partial^4 u_{p_0}}{\partial y^3 \partial x} +$$
$$w \frac{\partial^3 u_{p_0}}{\partial y^3} \frac{\partial u_{p_1}}{\partial x} + 3w \frac{\partial^2 u_{p_0}}{\partial y^2} \frac{\partial^2 u_{p_1}}{\partial x \partial y} + 3w \frac{\partial u_{p_0}}{\partial y} \frac{\partial^3 u_{p_1}}{\partial y^2 \partial x} +$$
$$w u_{p_0} \frac{\partial^4 u_{p_1}}{\partial y^3 \partial x} + w \frac{\partial^3 v_{p_1}}{\partial y^3} \frac{\partial u_{p_0}}{\partial y} + 3w \frac{\partial^2 v_{p_1}}{\partial y^2} \frac{\partial^2 u_{p_0}}{\partial y^2} +$$
$$3w \frac{\partial v_{p_1}}{\partial y} \frac{\partial^3 u_{p_0}}{\partial y^3} + w v_{p_1} \frac{\partial^4 u_{p_0}}{\partial y^4} + w \frac{\partial^3 v_{p_0}}{\partial y^3} \frac{\partial u_{p_1}}{\partial y} + 3w \frac{\partial^2 v_{p_0}}{\partial y^2} \frac{\partial^2 u_{p_1}}{\partial y^2} +$$
$$3w \frac{\partial v_{p_0}}{\partial y} \frac{\partial^3 u_{p_1}}{\partial y^3} + w v_{p_0} \frac{\partial^4 u_{p_1}}{\partial y^4} + \frac{\partial^3 u_{p_1}}{\partial y^3} + c_1 w \frac{\partial^2 u_{p_1}}{\partial y \partial t} +$$
$$c_1 w \frac{\partial u_{p_1}}{\partial y} \frac{\partial u_{p_0}}{\partial x} + c_1 w u_{p_1} \frac{\partial^2 u_{p_0}}{\partial x \partial y} + c_1 w \frac{\partial u_{p_0}}{\partial y} \frac{\partial u_{p_1}}{\partial x} +$$
$$c_1 w u_{p_0} \frac{\partial^2 u_{p_1}}{\partial y \partial x} + c_1 w \frac{\partial v_{p_1}}{\partial y} \frac{\partial u_{p_0}}{\partial y} + c_1 w v_{p_1} \frac{\partial^2 u_{p_0}}{\partial y^2} +$$
$$c_1 w \frac{\partial v_{p_0}}{\partial y} \frac{\partial u_{p_1}}{\partial y} + c_1 w v_{p_0} \frac{\partial^2 u_{p_1}}{\partial y^2} + c_1 \frac{\partial u_{p_1}}{\partial y} \quad (60)$$

The elimination of u_1 and v_1 from equations (44) and (45) and by using (38) and (43), yield the following equation:

$$w \frac{\partial^2 u_{p_1}}{\partial x \partial t} + w u_{p_1} \frac{\partial^2 u_{p_0}}{\partial x^2} + w \frac{\partial u_{p_1}}{\partial x} \frac{\partial u_{p_0}}{\partial x} + w \frac{\partial u_{p_0}}{\partial x} \frac{\partial u_{p_1}}{\partial x} +$$
$$w u_{p_0} \frac{\partial^2 u_{p_1}}{\partial x^2} + w \frac{\partial v_{p_1}}{\partial y} \frac{\partial u_{p_0}}{\partial y} + w v_{p_1} \frac{\partial^2 u_{p_0}}{\partial x \partial y} + w \frac{\partial v_{p_0}}{\partial x} \frac{\partial u_{p_1}}{\partial y} +$$
$$w v_{p_0} \frac{\partial^2 u_{p_1}}{\partial y^2} + w \frac{\partial^2 v_{p_1}}{\partial y \partial t} + w \frac{\partial u_{p_1}}{\partial y} \frac{\partial v_{p_0}}{\partial x} + w u_{p_1} \frac{\partial^2 v_{p_0}}{\partial y \partial x} +$$
$$w \frac{\partial u_{p_0}}{\partial y} \frac{\partial v_{p_1}}{\partial x} + w u_{p_0} \frac{\partial^2 v_{p_1}}{\partial y \partial x} + w \left(\frac{\partial v_{p_0}}{\partial y}\right)^2 + w v_{p_0} \frac{\partial^2 v_{p_0}}{\partial y^2} = 0 \quad (61)$$

After applying the normal mode analysis by substituting from Eq. (51) into Eqs. $(38)-(48)$, (60) and (61), the resulting ordinary differential equations may be solved exactly to give the following solutions:

$$u_{p_1}(x,y,t) = \left(k_{13} + k_{14} \sin\left(\sqrt{\frac{k_1}{k_2}} y\right) + k_{15} \cos\left(\sqrt{\frac{k_1}{k_2}} y\right) + c_{11} y \cos\left(\sqrt{\frac{k_1}{k_2}} y\right) + c_{12} \sin(c_1 y) + c_{13} y\right) e^{i\lambda(x-t)} \quad 62)$$

$$v_{p_1}(x,y,t) = \left(-i\lambda k_{13} y + i\lambda k_{14} \sqrt{\frac{k_2}{k_1}} cos\left(\sqrt{\frac{k_1}{k_2}} y\right) - i\lambda k_{15} \sqrt{\frac{k_2}{k_1}} sin\left(\sqrt{\frac{k_1}{k_2}} y\right) - i\lambda k_{16} - i\lambda \sqrt{\frac{k_2}{k_1}} c_{11} y \, sin\left(\sqrt{\frac{k_1}{k_2}} y\right) - i\lambda \sqrt{\frac{k_2}{k_1}} c_{11} \, cos\left(\sqrt{\frac{k_1}{k_2}} y\right) + \frac{i\lambda c_{12}}{\sqrt{c_1}} cos(\sqrt{c_1} y) - \frac{i\lambda c_{13}}{2} y^2\right) e^{i\lambda(x-t)} \quad (63)$$

$$u_1(x,y,t) = (c_{18} k_{14} \sin\left(\sqrt{\frac{k_1}{k_2}} y\right) + c_{18} k_{15} \cos\left(\sqrt{\frac{k_1}{k_2}} y\right) + k_{17} + k_{18} \sin(\sqrt{c_1} y) + k_{19} \cos(\sqrt{c_1} y) + c_{19} y \cos(\sqrt{c_1} y) + c_{20} \sin\left(\sqrt{\frac{k_1}{k_2}} y\right) + c_{21} y \cos(\sqrt{c_1} y) + c_{22} y) e^{i\lambda(x-t)} \quad (64)$$

$$v_1(x,y,t) = (-i\lambda k_{13} k_2 y + i\lambda k_{14} k_2 \sqrt{\frac{k_2}{k_1}} \cos\left(\sqrt{\frac{k_1}{k_2}} y\right) - i\lambda k_{15} k_2 \sqrt{\frac{k_2}{k_1}} \sin\left(\sqrt{\frac{k_1}{k_2}} y\right) - i\lambda k_{16} k_2 - i\lambda k_2 \sqrt{\frac{k_2}{k_1}} c_{11} y \sin\left(\sqrt{\frac{k_1}{k_2}} y\right) - i\lambda k_2 \sqrt{\frac{k_2}{k_1}} c_{11} \cos\left(\sqrt{\frac{k_1}{k_2}} y\right) + \frac{i\lambda c_{12} k_2}{\sqrt{c_1}} \cos(\sqrt{c_1} y) - \frac{i\lambda c_{13} k_2}{2} y^2) e^{i\lambda(x-t)} \quad (65)$$

$$\theta_1(x,y,t) = (k_{20} + k_{21} y) e^{i\lambda(x-t)} \quad (66)$$

$$\Omega_0(x,y,t) = (k_{22} + k_{23} y) e^{i\lambda(x-t)} \quad (67)$$

By introducing a stream function ψ_1 and as $u_1 = \frac{\partial \psi_1}{\partial y}$. (68)

This function ψ_1 and $\frac{\partial p_1}{\partial x}$ (from (55), (63) and (64) in (39)) may be evaluated numerically by using the Mathematica software.

The solutions for $u_p, v_p, u, v, \theta, \Omega$ and $\frac{\partial p}{\partial x}$ may be expressed by substituting from Eqs. $(52)-(59)$ and $(62)-(68)$ into Eq. (26) after neglecting the second and higher order terms of δ. The values of $(c_i : i = 1,2,3,\ldots,22)$ and $(k_i : i = 1,2,3,\ldots,23)$ are determined by utilizing the boundary conditions (35)–(37) and (46)–(48), and they are given in the Appendix.

4. RESULTS AND DISCUSSION

This section elucidates the behavior of streamlines configuration, fluid and particles velocity profile, pressure gradient, temperature profile and nanoparticle concentration of different involved parameters. In addition, it contains a comparison between the present results of the velocity by neglecting particle–fluid suspension when $\frac{L}{w} \ll 1$ and neglecting the effects of the Hall currents and ion slip when $\beta^* = \beta_i = \beta_e = 0$ with the previous results of Srinivas and Gayathri [25] which is considered as a special case of our work. The results are compared graphically in Fig. 2. The specific values in this figure are chosen as: $M = 3$; $k = 2$; $\lambda = 0.0007$; $\varepsilon = 0.155$; $Q = 0.1$; $\beta = 0.2$; $E_1 = 2$; $E_2 = 0.7$; $E_3 = 0.1$; $L = 0.001$; $w = 1$ and $\delta = 0.2$ in order to compare between the special cases (a) $\beta_* = \beta_i = \beta_e = 0$ and (b) $\beta_* = \beta_i = \beta_e = 0.01$. The figure gives an excellent matching between the present solutions and the previous ones. In addition, the results get more congruent when β^*, β_i and β_e approach to zero.

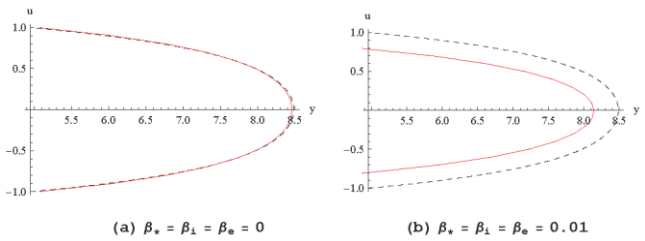

Fig .2 Plots of velocity $\boldsymbol{u}$ versus $\boldsymbol{y}$
(———) In the special case in our problem from Eqs. (26,54 and 64)
(-------) In previous results of S.Srinivas [25] (Fig.1 (d))

4.1. Streamlines configuration

The effect of the slip parameter β on the trapping is illustrated in Fig. 3. Also, Fig. 3 has the specific values $M = 0.3; k = 1.1; \lambda = 0.2; \varepsilon = 0.3; Q = 0.3; E_1 = 0.7; E_2 = 0.5; E_3 = 0.2; L = 2.; w = 0.8; \beta_* = 0.2; \beta_i = 0.5; \beta_e = 0.01$ and $\delta = 0.1$. It is observed that streamlines form closed loops, creating a cellular flow pattern in the channel and the trapped bolus decreases as the slip parameter β increases. The same effect of the slip parameter of the streamlines configuration was observed by Chaube et al. [28].

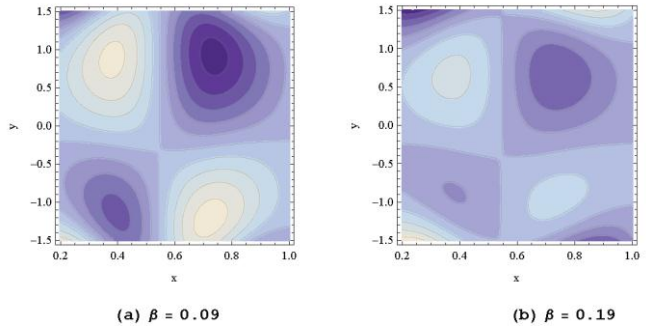

Fig .3 Plots of Streamline ψ distribution from Eqs. (26,59 and 68) for the effects of β

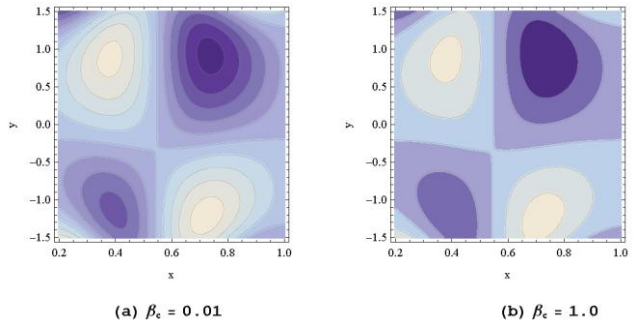

Fig .4 Plots of Streamline ψ distribution from Eqs. (26,59 and 68) for the effects of β_e

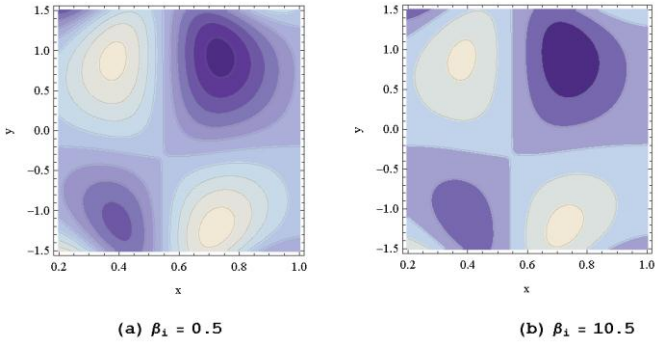

Fig .5 Plots of Streamline ψ distribution from Eqs. (26,59 and 68) for the effects of β_i

Fig. 4 and Fig. 5 highlights of the streamline patterns and trapping for the value of the Hall parameter β_e and ion-slip parameter β_i, respectively. All the physical parameters in Figs. 4, 5 are the same values of the parameters in Fig. 3 except β_e, β_i and at $\beta = 0.09$. It is observed that the trapped bolus decreases as the Hall parameter β_e and ion-slip parameter β_i are increased. The same behavior of the ion slip parameter was illustrated by Rafiq et al. [29].

4.2. The fluid and particle velocity profile

Figs. 6 and 7 have been plotted to show the implication of the slip parameter β on the fluid and particle velocity profiles. The particulars in these figures have the values $M = 1; k = 0.9; \lambda = 0.5; \varepsilon = 0.4; Q = 0.1; E_1 = 0.4; E_2 = 0.4; E_3 = 0.1; L = 0.7; w = 0.5; \beta_* = 0.3; \beta_i = 0.4; \beta_e = 0.3$ and $\delta = 0.2$. It is observed that the fluid velocity distribution increases with the increasing of β. This means that, under some conditions, urine in which solute particles are suspended (i.e., urine from a diseased kidney) is more susceptible to reversal flow in the ureter, in comparison to pure urine without solute particles. The same effect of the slip parameter on the fluid velocity profile was discussed by Kamel et al. [30]. This mechanism occurs since the resistance is reduced due to the deviation of fluid in a channel which enhances the fluid velocity profile (Fig. 6). In contrast, the particle velocity distribution, decreasing with the increasing of β. The same effect of the slip parameter on the fluid velocity profile was illustrated by Guria [31].

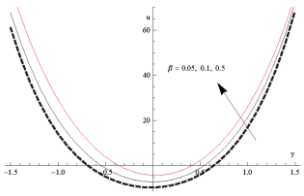

Fig .6 Plots of velocity u versus y from Eqs. (26,54 and 64) for the effects of β

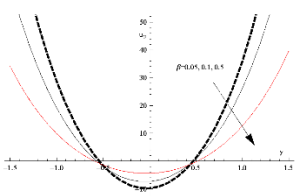

Fig .7 Plots of velocity u_p versus y from Eqs. (26,52 and 62) for the effects of β

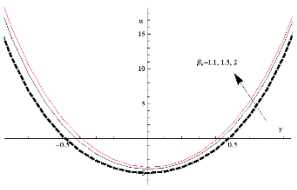

Fig .8 Plots of velocity u versus y from Eqs. (26,54 and 64) for the effects of β_e

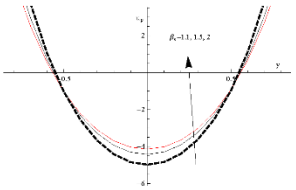

Fig .9 Plots of velocity u_p versus y from Eqs. (26,52 and 62) for the effects of β_e

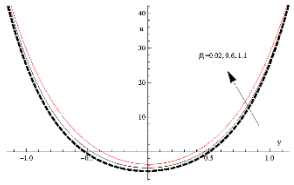

Fig .10 Plots of velocity u versus y from Eqs. (26,54 and 64) for the effects of β_i

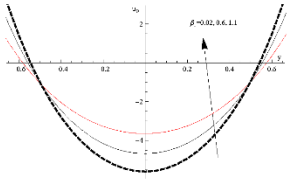

Fig .11 Plots of velocity u_p versus y from Eqs. (26,52 and 62)for the effects of β_i

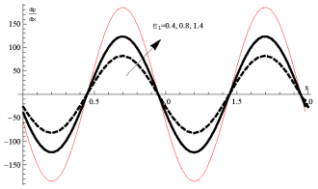

Fig .11 Plots of pressure gradient $\frac{dp}{dx}$ versus x from Eqs. (26,39 and 58) for the effects of E_1

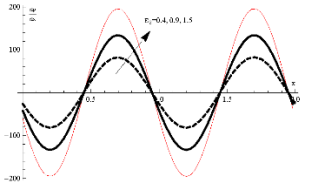

Fig .11 Plots of pressure gradient $\frac{dp}{dx}$ versus x from Eqs. (26,39 and 58) for the effects of E_2

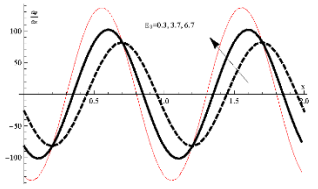

Fig .11 Plots of pressure gradient $\frac{dp}{dx}$ versus x from Eqs. (26,39 and 58) for the effects of E_3

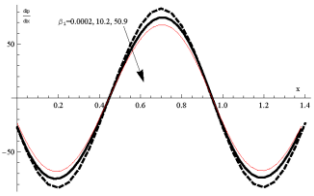

Fig .11 Plots of pressure gradient $\frac{dp}{dx}$ versus x from Eqs. (26,39 and 58) for the effects of β_i

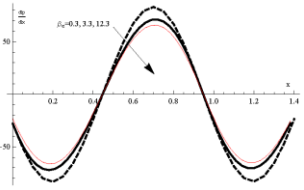

Fig .16 Plots of pressure gradient $\frac{dp}{dx}$ versus x from Eqs. (26,39 and 58) for the effects of β_e

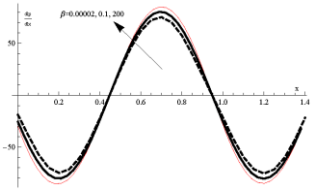

Fig .17 Plots of pressure gradient $\frac{dp}{dx}$ versus x from Eqs. (26,39 and 58) for the effects of β

It can be seen from Fig. 8 and Fig. 9 that larger Hall parameter values β_e increase the fluid and the particle velocity. This behavior physically holds as larger values of the conductivity β_e decreases which cause decay in the damping force and enhancement in the velocity [32]. The specific values in Fig. 8 are chosen as $M = 3; k = 0.4; \lambda = 0.5; \varepsilon = 0.4; Q = 0.1; \beta = 0.4; E_1 = 0.4; \quad E_2 = 0.4; E_3 = 0.1; L = 0.7; w = 0.5; \beta_* = 0.3; \beta_i = 0.4$ and $\delta = 0.2$. Figs. 9−11 are plotted at the same specific values of Fig. 8 except β_i and at $\beta_e = 1.1$.

Fig. 10 and Fig. 11 indicate that the increase of the magnitude of β_i increases the fluid and particle velocity. This behavior is physically occurring due to the decrease of the effective conductivity which decreases the damping force on the fluid and the particle velocity [33].

4.3. Pressure gradient profile

The impact of expanding coefficients E_1, E_2 and E_3 in Figs. 12 – 14 are to grow a quantity of pressure difference $\frac{dp}{dx}$ across the channel. Fig. 12 has the specific values $M = 2; k = 0.9; \lambda = 0.5; \varepsilon = 0.4; Q = 0.1; \beta = 0.4; E_2 = 0.4; E_3 = 0.1; L = 0.7; w = 0.5; \beta_* = 0.3; \beta_i = 0.4; \beta_e = 0.3$ and $\delta = 0.2$. The physical parameters in Figs. 13, 14 are the same values of the parameters in Fig. 12 except E_2, E_3 and at $E_1 = 0.4$. It is observed that, in the wider parts of the channel, the pressure gradient is small, that is, the flow can simply go without the burden of a great pressure gradient. Nonetheless, in the narrow parts of the channel, a lot bigger pressure gradient is needed to maintain the same flux to pass it. The same behavior for pressure difference across the channel was discussed by Ellahi et al. [34].

It is seen from Fig. 15 that in the narrow parts of the channel when an ion-slip parameter β_i Increases, the pressure gradient decrease, but in the wider parts of the channel, this behavior are the opposite. Also, Fig. 15 has the specific values $M = 1.2; k = 1.2; \lambda = 0.5; \varepsilon = 0.4; \quad Q = 0.1; \beta = 0.4; E_1 = 0.4; E_2 = 0.4; E_3 = 0.1; L = 0.7; w = 0.5; \beta_* = 0.3; \beta_e = 0.3$ and $\delta = 0.2$. Fig. 16 depicts that the pressure gradient is small when $x \in [0,0.5] \cup [1,1.5]$. Physically, it means that the flow can easily pass without any resistance of large pressure gradient. In this part, the pressure gradient increases with an increase in the Hall parameter β_e. However, in the narrow part of the channel when $x \in [0.5,1]$, a large pressure gradient is needed to maintain the same flux to pass through it. In this part, the pressure gradient decreases with an increase in a Hall parameter β_e [34]. Fig. 17 shows the effect of the slip parameter β on pressure gradient $\frac{dp}{dx}$. It is observed that the pressure gradient increases by the increase in β in the region $0.5 \leq x \leq 1$. At the same time, in the region $0 \leq x \leq 0.5$ and $1 \leq x \leq 1.5$, the contrary behavior is observed. We observed that through the narrowing part of the channel the flow cannot pass easily. Therefore, it requires a large pressure gradient to maintain the same flux to pass it in the narrow part of the channel. All the physical parameters in Figs. 16, 17 are the same values of the parameters in Fig. 15 except β_e, β and at $\beta_i = 0.0002$.

4.4. The temperature profile

Fig. 18 has been plotted to show the implication of the geometric parameters ε on the temperature profile θ. This Figure is plotted at the same specific values of Fig. 12 except ε and at $E_1 = 0.4$. It is seen that the temperature increases by the increase in ε in the region $0.1 \leq t \leq 0.6$. At the same time, in the region $0.6 \leq t \leq 1.1$, the contrary behavior is observed. This effect will be repeated periodically along with the increasing of time.

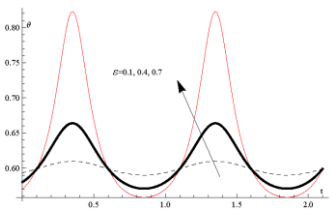

Fig .18 Plots of temperature profile θ versus t from Eqs. (26,56 and 66) for the effects of ε

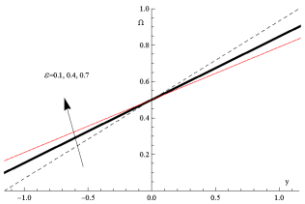

Fig .19 Plots of nanoparticle concentration Ω versus y from Eqs. (26,57 and 67) for the effects of ε

4.5. The nanoparticle concentration

It can be seen from Fig. 19 that the geometric parameter ε, tends to enhance the nanoparticle concentration Ω in the region $y \leq 0$, meanwhile, in the region $y \geq 0$ the opposite behavior is observed. This Figure is plotted for the same specific values of Fig. 12 except ε and at $E_1 = 0.4$.

5. CONCLUSION

The constitutive equations of motion, energy, and concentration are utilized to study the effects of the Hall currents, ion slip, slip conditions, together with the wall properties of a compressible flow on MHD peristaltic transport of a nanofluid with suspended particle–fluid through a porous medium. The normal modes analysis and a perturbation method together with the approximation of small Reynolds number, we're simplifying the governing equations. Approximate analytical solutions of the coupled partial differential equations were obtained. The main results can be epitomized in the following points:

1. The value of trapped bolus decreases with the increasing of the slip parameter β, the Hall parameter β_e, and ion-slip parameter β_i.
2. The fluid velocity u is an increasing function with the slip parameter β, the Hall parameter β_e and ion-slip parameter β_i.
3. The particle velocity u_p is an increasing function of the Hall parameter β_e and ion slip parameter β_i. In contrast, it decreases with the increasing of the slip parameter β.
4. The temperature profile increases with the increasing of ε in the region at $0.1 \leq t \leq 0.6$. Simultaneously, the opposite behavior is observed in the region at $0.6 \leq t \leq 1.1$. This effect is repeated periodically along with the increasing of time.
5. The nanoparticle concentration increases with the increasing of ε in the region $y \leq 0$, meanwhile, the opposite behavior is observed in the region $y \geq 0$.
6. The overwhelming effect of increasing E_1, E_2, E_3 and β are raising the magnitude of pressure difference $\frac{dp}{dx}$ across the channel. In contrast, decreasing β_e and β_i are reducing the magnitude of pressure difference $\frac{dp}{dx}$ across the channel.
7. Finally, a comparison was made between the present results of the fluid velocity and the previous results of Srinivas and Gayathri [25] (as a special case of the present article). The results were compared and comparisons showed an excellent compatible between the results.

Nomenclature

a	Amplitude.
B_0	Magnetic field.
C	Nanoparticle concentration.
C_0, C_1	Nanoparticle phenomena to the walls of the channel at $y = \eta$ and $-\eta$
C_v	Coefficient of viscous damping forces.
c_f	Volumetric volume expansion of the fluid.
c_p	Volumetric volume expansion of the particle.
c^*	Phase speed.
d	Mean half width of the channel.
Q^*, Q	Dimensional and non-dimensional non-uniformity of channel, respectively.
R	Reynolds number.
T_0, T_1	Temperatures to the walls of the channel at $y = \eta$ and $-\eta$
Sc	Schmidt number.
T	Temperature.
t	Time.
u, v	Components of fluid velocity along x-, y-directions.
u_p, v_p	Components of particle velocity along x-, y-directions.

D_B	Brownian diffusion coefficient.
D_T	Thermophoretic diffusion coefficient.
E_1, E_2, E_3	Non-dimensional elasticity parameters.
h	Dimensional slip parameter.
K	Permeability of the porous medium.
k	Thermal conductivity of the fluid.
L	The mass concentration of the particle.
M	Hartman number.
m_1^*	Mass per unit area.
m	The mass of a particle.
N_b	Brownian parameter.
N_t	Thermophoresis parameter.
p	Pressure.
p_0	Pressure on the outside surface of the wall due to the tension in the muscles.
Pr	Prandtl number.
w	The dimensionless relaxation time.

Greek symbols

β	Knudsen number (Slip parameter).
γ	The Stokes resistance coefficient.
ρ, ρ_p	Density of the fluid and the particle respectively.
ε, δ	Geometric parameters.
ζ	Number density
λ^*	Wavelength.
λ	Wave speed.
μ	Coefficient of viscosity of the fluid.
ν	Kinematic viscosity.
θ	Dimensionless temperature.
σ	Fluid electrical conductivity.
Ω	Dimensionless nanoparticle concentration.
β_i	The ion slip parameter.
β_e	The Hall parameter.
β^*	The Hall factor.
ψ	Stream function.

References

[1] Abbasi, F. M., Hayat, T., Ahmad, B. and Chen, G. Q., 2014, "Peristaltic motion of non-Newtonian nanofluid in an asymmetric channel," Verlag der Zeitschrift fur Naturforschung, 69a, pp. 451–461.

[2] Shehzad, S. A., Abbasi, F. M., Hayat, T. and Alsaadi, F., 2014, "MHD mixed convective peristaltic motion of nanofluid with Joule heating and thermophoresis effects," Plos One, 9 (11), e111417.

[3] Hayat, T., Abbasi, F. M., Al-Yami, M. and Monaquel, S., 2014, "Slip and joule heating effects in mixed convection peristaltic transport of nanofluid with Soret and Dufour effects," Journal of Molecular Liquids, 194, pp. 93–99.

[4] Khanafer, K., Vafai K. and Lightstone, M., 2003, "Buoyancy-driven heat transfer enhancement in a two dimensional enclosure utilizing nanofluids," International Journal of Heat and Mass Transfer, 46, pp. 3639–3653.

[5] Dong, S., Zheng, L., Zhang, X. and Lin, P., 2014, "Improved drag force model and its application in simulating nanofluid flow," Microfluidics and Nanofluidics, 17, pp. 253–261.

[6] Ullah Khan, S., Ali N. and Abbas, Z., 2016, "Influence of heat generation/absorption with convective heat and mass conditions in unsteady flow of Eyring Powell nanofluid over porous oscillatory stretching surface," Journal of Nanofluids, 5, pp. 351–362.

[7] Hayat, T., Imtiaz, M. and Alsaedi, A., 2015, "Impact of magnetohydrodynamics in bidirectional flow of nanofluid subject to second order slip velocity and homogeneous-heterogeneous reactions," Journal of Magnetism and Magnetic Materials, 395, pp. 294–302.

[8] Mekheimer Kh. S. and Elkot, M. A., 2010, "Suspension model for blood flow through arterial catheterization," Chemical Engineering Communications, 197, pp. 1195–1214.

[9] Mekheimer, Kh. S., El Shehawey E. F. and Elaw, A. M, 1998, "Peristaltic motion of a particle fluid suspension in a planar channel," International Journal of Theoretical Physics, 37, pp. 2895–2920.

[10] Hu, H. H., 1996, "Direct simulation of flows of solid-liquid mixtures.," International Journal of Multiphase Flow, 22, pp. 335–352.

[11] Feng, J. J., Huang P. and Joseph, D.D., 1996, "Dynamic simulation of sedimentation of solid particles in an Oldroyd-B fluid," Journal of Non-Newtonian Fluid Mechanics, 26, pp. 63–88.

[12] Abo-Eldahab, E. M., Barakat E. I. and Nowar, K. I., 2010, "Hall current and ion-slip effects on MHD peristaltic transport," International Journal of Applied Mathematics and Physics, 2, pp. 113–123.

[13] Srinivasacharya D. and Kaladhar, K., 2013, "Analytical solution for Hall and ion-slip effects on mixed convection flow of couple stress fluid between parallel disks," Mathematical and Computer Modelling, 57, pp.

2494–2509.

[14] Uddin Z. and Kumar, M., 2013, "Hall and ion-slip effect on MHD boundary layer flow of a micro polar fluid past a wedge," Scientia Iranica, 20, pp. 467– 476.

[15] Hayat, T., Zahir, H., Tanveer A. and Alsaedi, A., 2016, "Influences of Hall current and chemical reaction in mixed convective peristaltic flow of Prandtl fluid," Journal of Magnetism and Magnetic Materials, 407, pp. 321–327.

[16] Kwang, W., Chu H. and Fang, J., 2000, "Peristaltic transport in a slip flow," The European Physical Journal B., 16, pp. 543–547.

[17] Abedin, A., Arash K. and Davood, T., 2018, "Investigation into the effects of slip boundary condition on nanofluid flow in a double-layer microchannel," Journal of Thermal Analysis and Calorimetry, 131, pp. 2975–2991.

[18] Soltani F. and Yilmazer, Ü., 1998, "Slip velocity and slip layer thickness in flow of concentrated suspensions," Journal of Applied Polymer Science, 70 (3), pp. 515–522.

[19] Hayat, T., Nisar, Z., Ahmad B. and Yasmin, H., 2015, "Simultaneous effects of slip and wall properties on MHD peristaltic motion of nanofluid with Joule heating," Journal of Magnetism and Magnetic Materials, 394, pp. 48–58.

[20] Shahzadi, I., Sadaf, H., Nadeem S. and Saleem, A., 2017, "Bio-mathematical analysis for the peristaltic flow of single wall carbon nanotubes under the impact of variable viscosity and wall properties," Computer methods and programs in biomedicine, 139, pp. 137–147.

[21] Singhal R. and Srivastava, K. M., 1948, "Thermal oscillations of a particle fluid mixture with horizontal temperature gradient," Applied Scientific Research, 41, pp. 155–166.

[22] Crammer, K. R, 1973, "Magnetofluid dynamics for engineers and applied physicists," Electrical Engineering in Japan, 93(1), pp. 142–142.

[23] Sutton G. W. and Sherman, A., 1965, "Engineering Magnetohydrodynamics," New York, McGraw-Hill.

[24] Mittra T. K. and Prasad, S. N., 1973, "On the influence of wall properties and Poiseuille flow in peristalsis," Journal of Biomechanics, 6, pp. 681−691.

[25] Srinivas, S., Gayathri R. and Kothandapani, M., 2009, "The influence of slip conditions, wall properties and heat transfer on MHD peristaltic transport," Computer Physics Communications, 180, pp. 2115–2122.

[26] Fung Y. C. and Yih, C. S., 1968, "Peristaltic transport," Journal of Applied Mechanics, 35, pp. 669-675.

[27] Fung Y. C. and Yin, F., 1969, "Peristaltic waves in circular cylindrical tubes," Journal of Applied Mechanics, 36, pp. 579–587.

[28] Chaube, M. K., Pandey S. K. and Tripathi, D., 2010, "Slip effect on peristaltic transport of micropolar fluid," Applied Mathematical Sciences, 4 (43), pp. 2105–2117.

[29] Rafiq, M., Yasmin, H., Hayat T. and Alsaadi, F., 2019, "Effect of Hall and ion-slip on the peristaltic transport of nanofluid: A biomedical application," Chinese Journal of Physics, 60, pp. 208–227.

[30] Kamel, M. H., Eldesoky, I. M., Maher B. M. and Abumandour, R. M, 2015, "Slip effects on peristaltic transport of a particle-fluid suspension in a planar channel," Applied Bionics and Biomechanics, 2015, pp. 1–14.

[31] Guria, M., 2016, "Effect of slip condition on vertical channel flow in the presence of radiation," International Journal of Applied Mechanics and Engineering, 21, pp. 341–358.

[32] Hayat, T., Asghar, S., Tanveer A. and Alsaedi, A., 2019, "Effects of Hall current and ion-slip on the peristaltic motion of couple stress fluid with thermal deposition," Neural Computer and Application, 31, pp. 117–126.

[33] Hazem Ali, A., 2014, "Ion slip effect on the flow due to a rotating disk," Arabian Journal for Science and Engineering, 29, pp. 165–172.

[34] Ellahi, R., Bhatti M. M. and Pop, I., 2016, "Effects of hall and ion slip on MHD peristaltic flow of jeffrey fluid in a non-uniform rectangular duct," International Journal of Numerical Methods for Heat and Fluid Flow, 26, pp. 1802–1820.

Appendix

The Appendix is too large to add in text, so it is obtained to the journal to add it.